WILEY | Hindawi

Research Article

Levenberg–Marquardt Backpropagation for Numerical Treatment of Micropolar Flow in a Porous Channel with Mass Injection

Hakeem Ullah [ID],[1] **Imran Khan,**[1] **Hussain AlSalman** [ID],[2] **Saeed Islam,**[1] **Muhammad Asif Zahoor Raja** [ID],[3] **Muhammad Shoaib,**[4] **Abdu Gumaei** [ID],[5] **Mehreen Fiza,**[1] **Kashif Ullah,**[1] **Sk. Md. Mizanur Rahman,**[6] **and Muhammad Ayaz**[1]

[1]*Department of Mathematics, Abdul Wali Khan University Mardan, Mardan, KP 23200, Pakistan*
[2]*Department of Computer Science, College of Computer and Information Sciences, King Saud University, Riyadh 11543, Saudi Arabia*
[3]*Future Technology Research Center, National Yunlin University of Science and Technology, 123 University Road, Section 3, Douliou, Yunlin 64002, Taiwan*
[4]*Department of Mathematics, COMSATS University Islamabad, Attock Campus, Attock 43600, Pakistan*
[5]*Department of Computer Science Faculty of Applied Sciences, Taiz University, Taiz 6803, Yemen*
[6]*Information and Communication Engineering Technology, School of Engineering Technology and Applied Science, Centennial College, Toronto, Canada*

Correspondence should be addressed to Hakeem Ullah; hakeemullah1@gmail.com and Abdu Gumaei; abdugumaei@taiz.edu.ye

In this research work, an effective Levenberg–Marquardt algorithm-based artificial neural network (LMA-BANN) model is presented to find an accurate series solution for micropolar flow in a porous channel with mass injection (MPFPCMI). The LMA is one of the fastest backpropagation methods used for solving least-squares of nonlinear problems. We create a dataset to train, test, and validate the LMA-BANN model regarding the solution obtained by optimal homotopy asymptotic (OHA) method. The proposed model is evaluated by conducting experiments on a dataset acquired from the OHA method. The experimental results are obtained by using mean square error (MSE) and absolute error (AE) metric functions. The learning process of the adjustable parameters is conducted with efficacy of the LMA-BANN model. The performance of the developed LMA-BANN for the modelled problem is confirmed by achieving the best promise numerical results of performance in the range of E-05 to E-08 and also assessed by error histogram plot (EHP) and regression plot (RP) measures.

1. Introduction

A few years ago, Eringen [1, 2] firstly presented the idea of micropolar fluids. Theories of non-Newtonian fluid are developed to describe the behavior of the fluid that does not obey Newton's law, such as micropolar fluids. This fluid summarizes specific non-Newtonian behaviors, such as liquid with polymer additives, liquid crystals, animal blood particles, suspensions, and topographic features. The governing equations of many physical problems are nonlinear in

nature and cannot be solved analytically; therefore, the scientist developed some approximate and numerical techniques, such as perturbation-based methods [3, 4], homotopy perturbation-based methods [5–7], homotopy analysis-based methods [8–10], collocation-based method [11–18], and Adomian decomposition-based methods [19, 20]. Among these methods, artificial intelligence (AI)-based numerical methods have been broadly designed for solving differential equations in several diverse applications [21–23]. A few latest research works to solve the problems of

nonlinear systems include the study introduced for local fractional partial differential equations [24], fourth-order nonlinear differential equations [25], Riccati equation control of nonlinear uncertain systems [26], analytic solution of micropolar flow using the homotopy analysis method [27], and pantograph delay differential equation [28]. However, these numerical-based methods need discretization and improved linearization techniques, which only allow computing the solution for certain standards variables and required huge computer memory and time. For optimizing the results, convergence and stability should be considered to avoid divergence. The perturbative methods required the assumption of small parameters, which is itself an issue. Besides, there is no study yet has been applied a fast backpropagation method for finding an accurate series solution to micropolar flow in a porous channel with mass injection (MPFPCMI).

Therefore, the aim of this study is to develop a Levenberg–Marquardt algorithm-based artificial neural network (LMA-BANN) model to solve the nonlinear governing equation of MPFPCMI. The contributions and mechanisms of the proposed work fall under following points:

(i) The LMA-BANN model is developed to analyze MPFPCMI for diverse scenarios on variants of physical parameters.

(ii) The dataset for LMA-BANN is obtained by variations of different parameters with the help of the OHA method.

(iii) The validity and accuracy of LMA-BANN are confirmed by comparing its results at different cases and scenarios. The results of training, testing, and validation are subjected by displaying the MPFPCMI for diverse scenarios.

(iv) The MSE metric function, EHP, and RP results are obtained with the help of plots to show the performance of LMA-BANN for finding an accurate series solution of MPFPCMI successfully.

2. Problem Formulations

Consider the steady, incompressible, and laminar flow of micropolar fluid along two-dimensional channel with porous walls. The mass fluid is introduced with speed q. The walls of the channel are adjusted at $y = \pm h$, where $2h$ is the width of the channel [29, 30]. The fundamental equations governing are as follows [31, 32]:

$$\underset{\sim}{u}_x + \underset{\sim}{v}_y = 0, \tag{1}$$

$$\underset{\sim}{u}\,\underset{\sim}{u}_x + \underset{\sim}{v}\,\underset{\sim}{u}_y = -\frac{1}{\rho}p_x + \left(v + \frac{k}{\rho}\right)\left(\underset{\sim}{u}_{xx} + \underset{\sim}{u}_{yy}\right) + \frac{k}{\rho}N_x, \tag{2}$$

$$\underset{\sim}{u}\,\underset{\sim}{v}_x + \underset{\sim}{v}\,\underset{\sim}{v}_y = -\frac{1}{\rho}p_y + \left(v + \frac{k}{\rho}\right)\left(\underset{\sim}{v}_{xx} + \underset{\sim}{v}_{yy}\right) - \frac{k}{\rho}N_x, \tag{3}$$

$$\underset{\sim}{u}\,N_x + \underset{\sim}{v}\,N_y = -\frac{1}{\rho j}\left(2N + \underset{\sim}{u}_y - \underset{\sim}{v}_x\right) + \frac{v_s}{\rho j}\left(N_{xx} + N_{yy}\right). \tag{4}$$

The suitable conditions for physical boundaries are as follows [26, 27]:

$$\underset{\sim}{u}\,(x, \pm h) = 0,$$

$$\underset{\sim}{v}\,(x, \pm h) = \pm q, \tag{5}$$

$$N\,(x, \pm h) = -s\underset{\sim}{u}_y|_{(x, \pm h)}.$$

The symmetric flow (SF) is as follows [33]:

$$\underset{\sim}{u}_x(x, 0) = 0,$$

$$\underset{\sim}{v}\,(x, 0) = 0. \tag{6}$$

Here, q greater than zero relates to suctions, q less than zero corresponds to injections, and "s" is a finite-parameters worn to model the degree to which microelements in the region of the channel walls are free to rotate, e.g., as "s" is equal to zero is the case where microelements near the boundary cannot turn around when $s = 0.5$, the situation of microrotation is identical to the velocity of the fluid at the end. Kelson et al. [29] developed the following equations:

$$\phi = -qx\,\underset{\sim}{f}\,(\eta).$$

$$N = \frac{qx}{h^2}\,\underset{\sim}{g}(\eta), \tag{7}$$

where

$$\eta = \frac{y}{h},$$

$$\underset{\sim}{u} = \phi_y$$

$$= -\frac{qx}{h}f'(\eta), \tag{8}$$

$$\underset{\sim}{v} = -\phi_x = \eta f(\eta).$$

The Navier–Stokes equations (1)–(4) decrease via applying equations (7) and (8):

$$(1 + N_1)\overset{iv}{\underset{\sim}{f}} - N_1\,\underset{\sim}{g}'' - \text{Re} \times \left(\underset{\sim}{f}\,\underset{\sim}{f}''' - \underset{\sim}{f}'\,\underset{\sim}{f}''\right) = 0,$$

$$N_2\,\underset{\sim}{g}'' + N_1\left(\underset{\sim}{f}'' - 2\,\underset{\sim}{g}\right) - N_3\text{Re}\left(\underset{\sim}{f}\,\underset{\sim}{g}' - \underset{\sim}{f}'\,\underset{\sim}{g}\right) = 0. \tag{9}$$

Dimensionless parameters are established as follows:

$$N_1 = \frac{k}{\rho v},$$

$$N_2 = \frac{v_s}{\rho v h^2},$$

$$N_3 = \frac{j}{h^2}, \tag{10}$$

$$\text{Re} = \frac{qh}{v}.$$

When viscosity parameter (Re) is more significant than zero used for suction and less than for injection, the BCs are

$$\underset{\sim}{f}(\pm 1) = 1,$$

$$\underset{\sim}{f}'(\pm 1) = 0, \tag{11}$$

$$\underset{\sim}{g}(\pm 1) = s \times \underset{\sim}{f}''(\pm 1).$$

The SF is as follows:

$$\underset{\sim}{f}(0) = 0,$$

$$\underset{\sim}{f}''(0) = 0,$$

$$\underset{\sim}{f}'(1) = 0, \tag{12}$$

$$\underset{\sim}{f}(1) = 1,$$

$$\underset{\sim}{g}(1) = s \times \underset{\sim}{f}''(1).$$

By applying Kelson et al. [29], we put $s = 0$, $N_1 = 1, N_2 = 1,$ and $N_3 = 0.1$:

$$2\overset{iv}{\underset{\sim}{f}} - \text{Re}\,\underset{\sim}{f}\,\underset{\sim}{f}''' = -\text{Re}\,\underset{\sim}{f}'\,\underset{\sim}{f}'' + \underset{\sim}{g}'', \tag{13}$$

$$\underset{\sim}{g}'' + \underset{\sim}{f}'' - 0.1\text{Re}\,\underset{\sim}{f}\,\underset{\sim}{g}' = 0.1\text{Re}\,\underset{\sim}{f}'\,\underset{\sim}{g} + 2\underset{\sim}{g}. \tag{14}$$

The BCs are as follows:

$$\underset{\sim}{f}(0) = 0,$$

$$\underset{\sim}{f}''(0) = 0,$$

$$\underset{\sim}{f}'(1) = 0,$$

$$\underset{\sim}{f}(1) = 1, \tag{15}$$

$$\underset{\sim}{g}(1) = 0,$$

$$\underset{\sim}{g}(0) = 0.$$

3. Numerical Experimental Results with Discussion

A short overview of the scheme proposed for finding the proposed LMA-BANN numerical experimentation continuity and momentum equations, i.e., 2–4, based on MPFPCMI is accessible in this section. The proposed structure of stepwise flow is presented in Figure 1 by using "nftool" of the NN tool-box existed in MATLAB. LMA-BANN is implemented for two-layer structures that include single input hidden and output of feed-forward network by LMA-based backpropagation process. Figure 2 demonstrates the structural design of ANN based on ten neuron numbers with a data-sigmoid activation function.

A reference dataset for LMA-BANN for equations (14) and (15) is created between intervals [0, 1] for 201 input grids. Now, 80 percent of data are used for training as 10 percent is for testing and 10 percent is for validation in the event of a 2-layer feed-forward ANN structure fitting tool with LMA backpropagation to solve all problems of MPFPCMI. Training data are used to establish the estimated solution on the source of the MSE, validation data are used to LMA-BANN, and even as test data are used to assess the truthful input performance.

Figures 3 and 4 show the effects of LMA-BANN performance represented by error histograms and fitting of solutions for two cases of the MPFPCMI scenario, while the regression tests are shown in Figure 5 for two cases of the MPFPCMI scenario. Furthermore, the MSE, number epochs, and other convergence parameters for training, validation, and testing data are tabulated in Tables 1 and 2, for two cases of the MPFPCMI scenario. Also, in Figures 3(a) and 3(c) of the MPFPCMI scenario, the convergence of MSE for the train, validation, and test process is provided for the two cases of the MPFPCMI. The best network performance for different scenarios is $9.889E - 13$ at 110 epochs and $9.889E - 13$ at 110 epochs. The gradient and step-size Mu of backpropagation nearly [9.8879×10^{-08} and 9.8879×10^{-08}] and [10^{-11}, 10^{-11}] are as shown in Figures 3(b) and 3(d). The results indicate the exact and convergent output for each case of the LMA-BANN.

The result obtained by LMA-BANN is achieved with the numerical outcome of the OHA method for two cases scenario, and the outcomes are shown in Figures 4(b) and 4(d) with the input points between {0–1} and step-size 1/100. The considerable error attained for training, testing, and validation statistics by planned ANN-LMM is less than 0.9×10^{-06} and -0.9×10^{-06} for the two cases of the scheme design. For each input stage, the error dynamics are further evaluated by error histograms, and results are given in Figures 4(a) and 4(c) for two cases of the MPFPCMI scenario. The error with 20-bin is nearly $-1.4E - 08$ and $-1.4E - 08$ for scenarios of MPFPCMI.

The outcomes for solving the LMA-BANN for different scenarios are shown in Tables 1 and 2, respectively. The output of LMA-BANN is about 10^{-13} to 10^{-12} and 10^{-10} to 10^{-11} for scenarios of MPFPCMI. The reliable output of
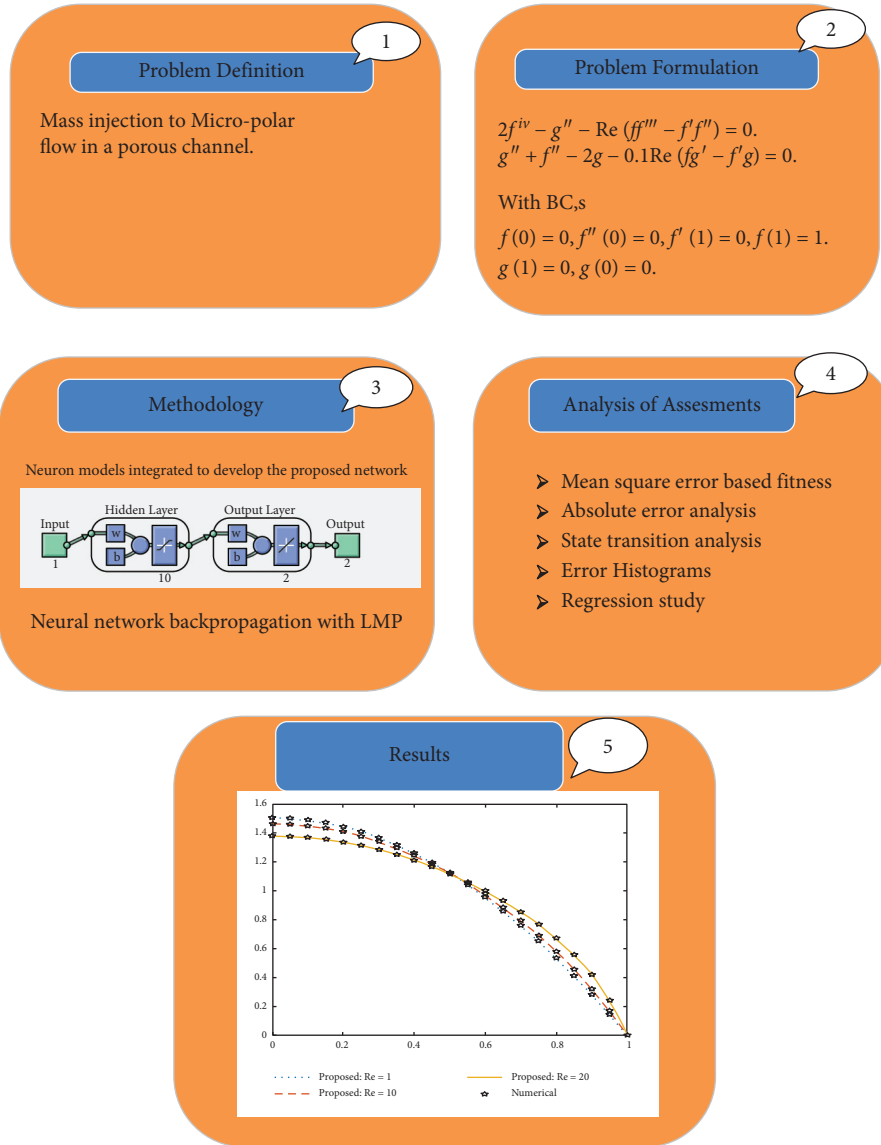
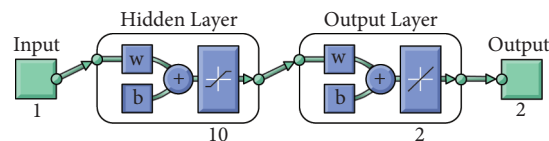FIGURE 1: Process workflow of proposed LMA-BANN for MPFPCMI.

FIGURE 2: Neural network model architecture.

LMA-BANN for explaining MPFPCMI is illustrated in these results. The results of LMA-BANN for the velocity and the profiles for the scenarios are therefore calculated. The experimental results of LMA-BANN are obtained for the velocity profiles $f(\eta), f'(\eta)$, and $g(\eta)$ of the adopted scenarios. The outcomes of $f(\eta), f'(\eta)$, and $g(\eta)$ profiles are shown in Figures 6–8 of the three scenarios of the MPFPCMI. Increasing the value of Re increases the velocity in x-direction and mass injection. The order to access the correctness gauges, the outcomes of LMA-BANN matched with the OHA method solutions in situations, and absolute errors (AEs) with references are calculated, and results are displayed in Figures 6(b), 7(b), and 8(b) for the three scenarios of the MPFPCMI. The AE is about 10^{-05} to 10^{-04}, 10^{-06} to 10^{-07}, 10^{-04} to 10^{-07}, 10^{-05} to 10^{-04}, 10^{-05} to 10^{-06}, 10^{-06} to 10^{-08}, 10^{-06} to 10^{-04}, 10^{-05} to 10^{-06}, and 10^{-05} to 10^{-06} for Re = 1, Re = 6, and Re = 20 and Re = 1, Re = 10, and Re = 20 of the scenarios. All these numerical and also graphical figures validated the reliable, convergent, and effective relationship of the LMA-BANN computing
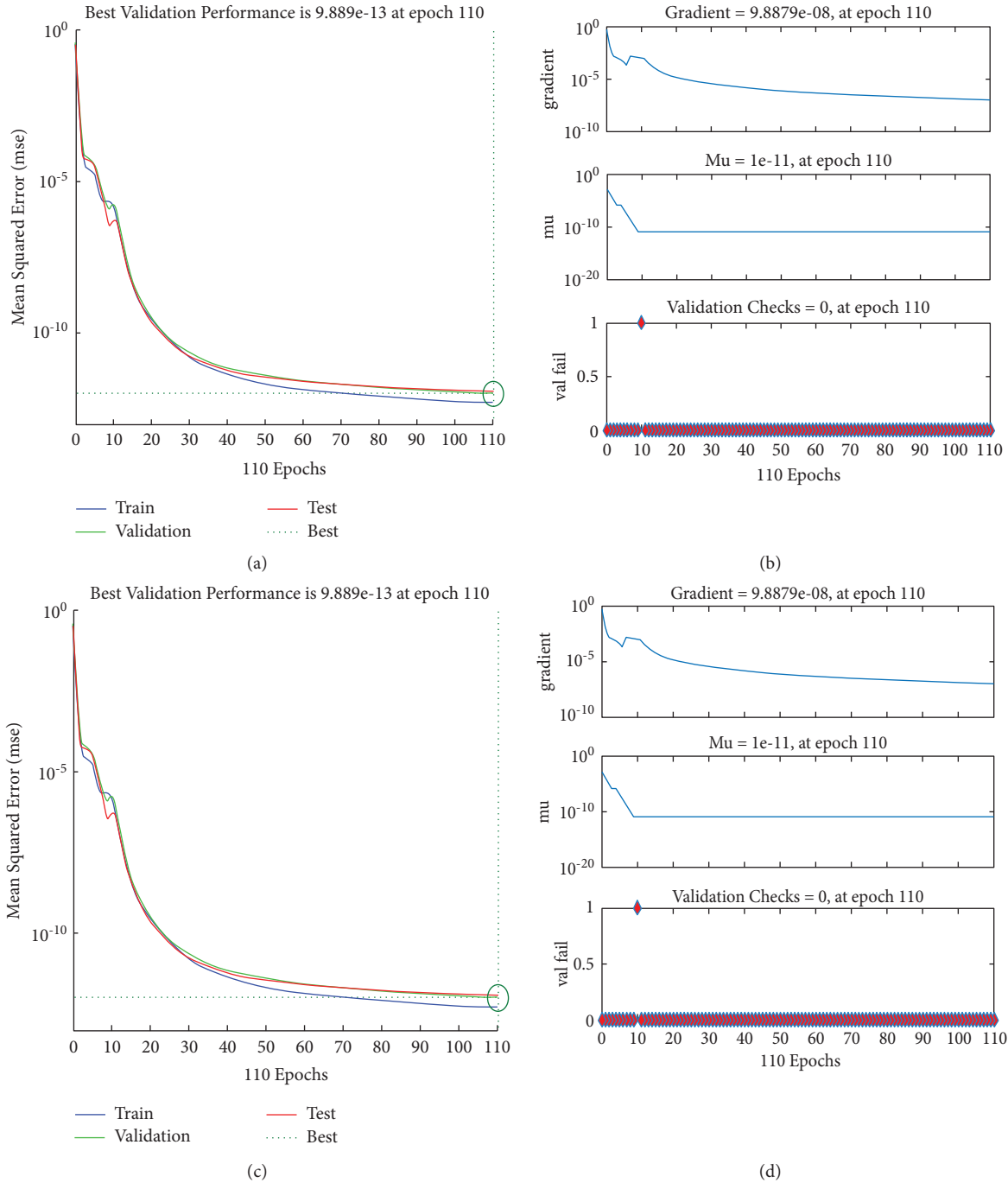
(a)

(b)

(c)

(d)

FIGURE 3: The performance and MSE outcomes of LMA-BANN in two cases of the MPFPCMI scenario.

approach for solving the variants of MPFPCMI. In Figure 7(a), the special effects of the Reynolds numbers on the profile of the velocity index are presented. For the velocity index $f(\eta)$, the Reynolds numbers increase with increasing the velocity index $f(\eta)$ of the injection case. The direct effect of the Reynolds number on the rotation profile of the fluid is presented in Figure 8(a). By increasing the Reynolds number, the rotational profile index of the fluid flow reduces up to $\eta = 0.6$, and then the rotation profile increases with the increase in the Reynolds number.

Increasing the Reynolds number with a minimum rotation occurred does not make it move away from the origin of the channel.

According to the results in Table 1, we can see that the model achieves the values $2.07665E - 12$, $4.16509E - 9$, and $2.3595E - 10$ of the MSE on the test data for cases 1, 2, and 3, when the number of epochs are 121, 214, and 223, respectively. We notice that all these values of the MSE are too low, confirming the effectiveness of the model. However, the lowest value is obtained for case 1 at the smallest value of
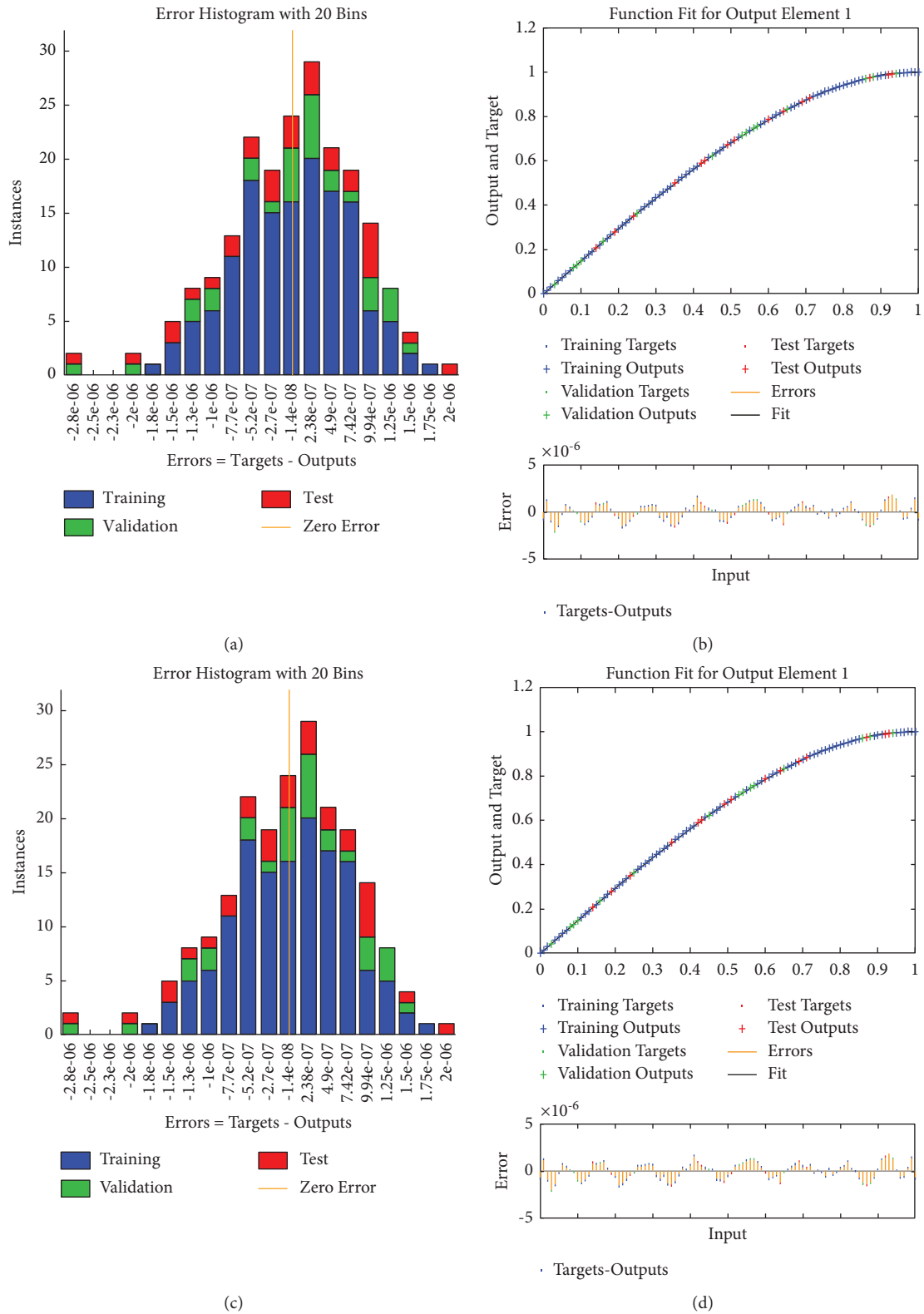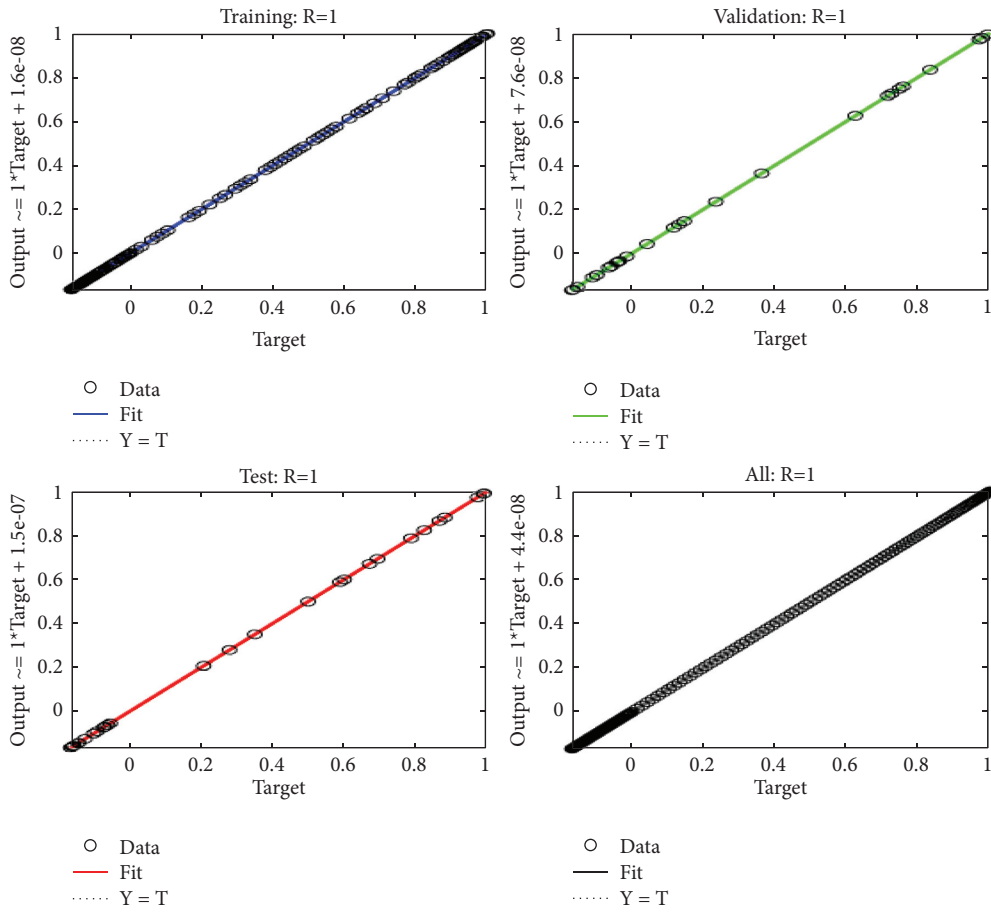
(a)

(b)

(c)

(d)

FIGURE 4: Outcomes of error histograms and fitting graphs of proposed LMA-BANN in two cases of the MPFPCMI scenario.
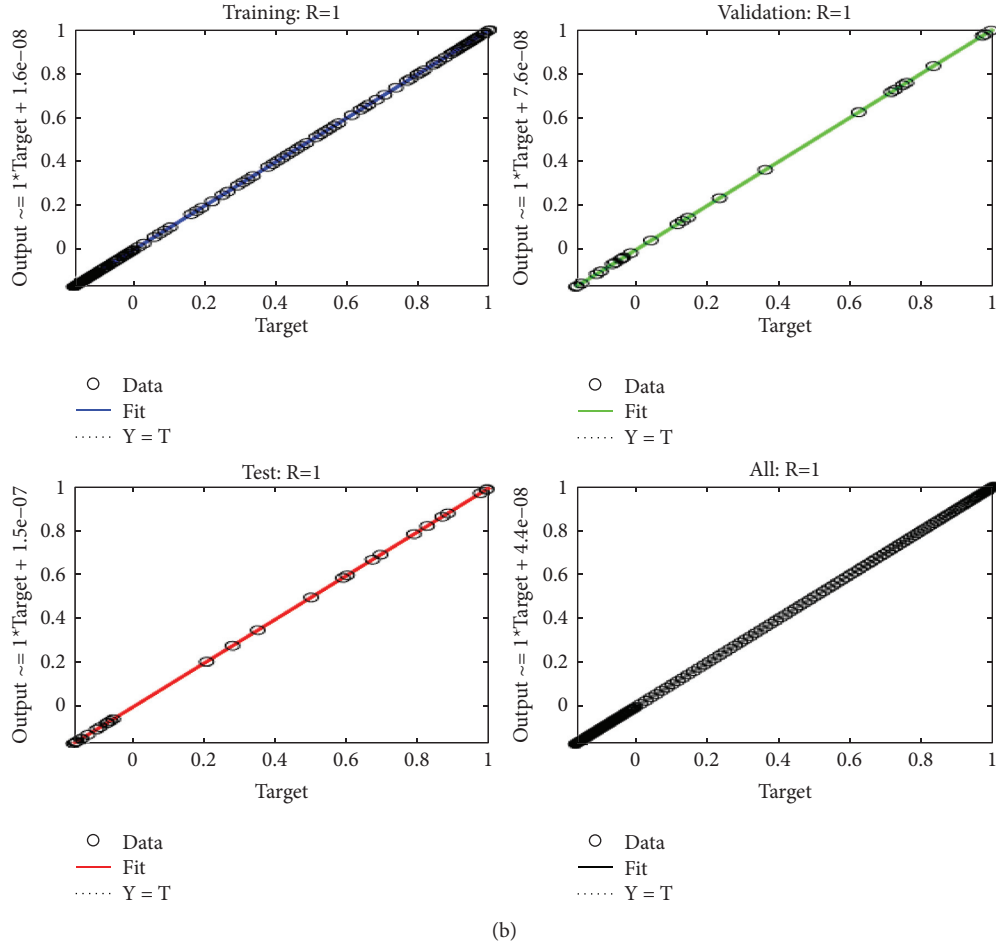
(a)

FIGURE 5: Continued.

(b)

Figure 5: Regression plot of LMA-BANN for two cases of the MPFPCMI scenario.

Table 1: Data of LMA-BANN for scenario 1 of the MPFPCMI.

Case	MSE			Performance	Gradient	Mu	Epoch
	Training	Validation	Testing				
1	$4.77038E-13$	$1.07665E-12$	$2.07665E-12$	$4.77E-13$	$9.83E-08$	$1.00E-11$	121
2	$3.31283E-11$	$1.53447E-10$	$4.16509E-9$	$3.31E-11$	$9.96E-08$	$1.00E-09$	214
3	$7.61638E-12$	$1.95429E-9$	$2.3595E-10$	$7.57E-12$	$9.84E-08$	$1.00E-10$	123

Table 2: Data of LMA-BANN for scenario 2 of the MPFPCMI.

Case	MSE			Performance	Gradient	Mu	Epoch
	Training	Validation	Testing				
1	$5.40353E-10$	$1.0355E-9$	$1.08132E-9$	$5.40E-10$	$9.95E-08$	$1.00E-09$	92
2	$3.93472E-10$	$7.23124E-10$	$4.7336E-10$	$3.93E-10$	$1.00E-07$	$1.00E-08$	329
3	$4.45013E-11$	$5.86838E-11$	$8.78423E-11$	$4.45E-11$	$9.90E-08$	$1.00E-09$	177

epoch's number. In addition, from the results in Table 2, it obvious that the model gets the values $1.08132E-9$, $4.7336E-10$, and $8.78423E-11$ for the test data at epoch's number 92, 329, and 177 and through the settings of case 1, case 2, and case 3. The lowest value is obtained for case 3 at

epoch's number 177, which is also an acceptable number of epochs. This also confirms the efficiency of the LMA-BANN model. Finally, from Figures 6(b)–8(b), we can see that lowest values of error plot are for Re = 10 for all scenarios, which means that this value is suitable for Re parameter.

(a)

(b)

FIGURE 6: Evaluation of proposed LMA-BANN with the numerical reference results for the MPFPCMI scenario 1: (a) outcomes for different value of Re in f; (b) error plot of Re in f.

(a)

(b)

FIGURE 7: Evaluation of proposed LMA-BANN with the numerical reference results for the MPFPCMI scenario 2: (a) outcomes for different value of Re in g; (b) error plot of Re in velocity g.

(a)

(b)
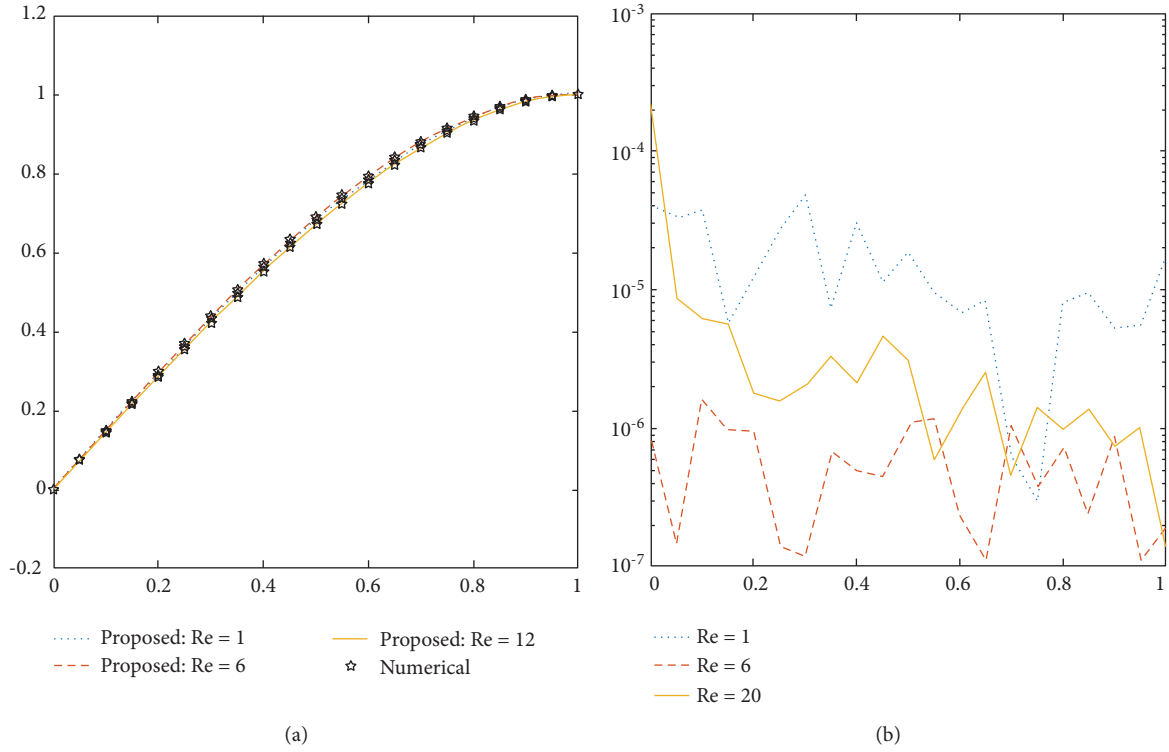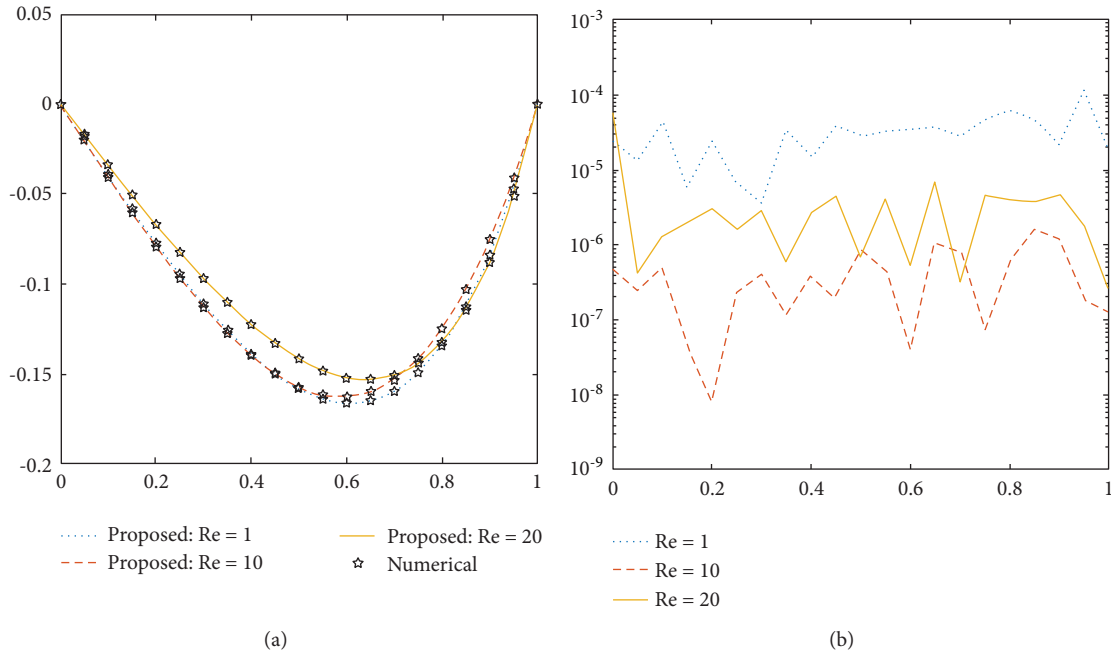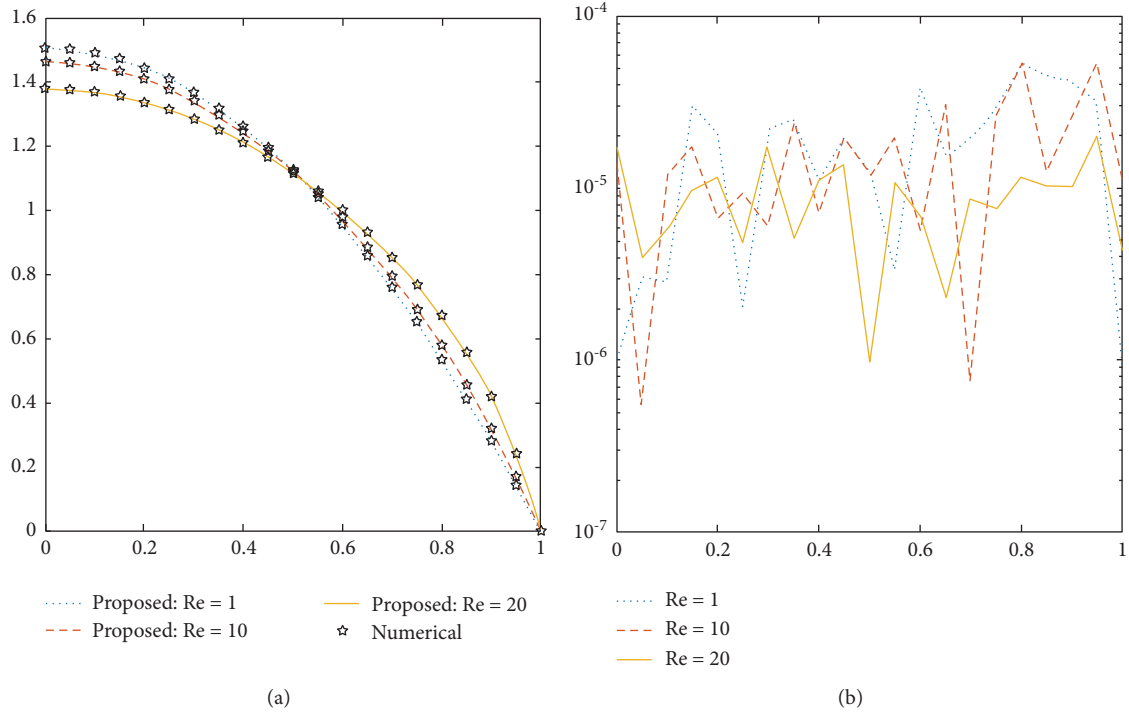
FIGURE 8: Evaluation of proposed LMA-BANN with the numerical reference results for the MPFPCMI scenario 3: (a) outcomes for different value of Re in *f*; (b) error plot of Re in velocity *f*.

4. Conclusion

The LMA-BANN is used as an artificial intelligence-based integrated method to find an accurate series solution for the MPFPCMI. The partial differential equations (PDEs) system of the MPFPCMI is converted to the order differential equations (ODEs) system by using the ability of similarity variables. The OHA method is used for producing the dataset of the MPFPCMI. Different measurable quantity of a set of metrics is utilized for evaluating the developed model. For training the model, a percentage equals to 80% of the data used, and a percentage of 10% from the remaining is used for testing, as well as the last 10% of the reference data is applied for validating the LMA-BANN model. The near values of both planned and reference outcomes matching of level between 10^{-05} to 10^{-07} confirm the rightness of solution, and supposed feature is additional authentic via numerical and graphical design of for the convergence of MSE, AE, error histogram plot, and regression plot measures. After this assurance, the results are demonstrated for the rotating and velocity profile when there are different values of Reynolds number and viscosity parameter (Re). From the numerical results of the problem, we get that increasing the value of Re decreases the velocity in x-direction and mass injection. Moreover, the experimental results confirmed the effectiveness of the LMA-BANN model for accurate analysis of MPFPCMI. In future work, we plan to apply the designed model for finding a solution to another nonlinear system with a large dataset and with different percentages of testing for more analyzing and investigating.

Abbreviations

$\widetilde{B}$:	Magnetic field (NmA^{-1})
C:	Fluid concentration
c_p:	Specific heat (J/kgK)
β:	Non-Newtonian parameter
$\widetilde{E}$:	Electric field intensity (NC^{-1})
J_w:	Mass flux
$\alpha_1, \alpha_2, \beta_1, \beta_2, \beta_3$:	Material constants
A_1, A_2, A_3:	Kinematic tensors
k:	Thermal conductivity $(\text{Wm}^{-1}\text{K}^{-1})$
M:	Magnetic parameter
n_e:	Number density of electron
O:	Origin
P:	Fluid pressure (Pa)
Pr:	Prandtl number
Q_w:	Heat flux (Wm^{-2})
q_r:	Radioactive heat flux (J)
Re:	Viscosity parameter
S:	Cauchy stress tensor
t_e:	Flow time (s)
T:	Fluid temperature (K)
u, v, w:	Velocities components (ms^{-1})
x, y, z:	Coordinates.

Greek Letters

α:	Thermal diffusivity $(\text{m}^2\text{s}^{-1})$
$\widehat{\kappa}$:	Vertex viscosity (mPa)
μ:	Dynamic viscosity (mPa)
v:	Kinematic coefficient of viscosity

ρ_f: Base fluid density (Kgm^{-3})
ρ_b: Density of the particles (Kgm^{-3}).

Data Availability

All the relevant data are included within the manuscript.

Conflicts of Interest

The authors declare that there are no conflicts of interest about the publication of the research article.

Acknowledgments

References

[1] A. C. Eringen, "Simple microfluids," *International Journal of Engineering Science*, vol. 2, no. 2, pp. 205–217, 1964.

[2] A. Eringen, "Theory of micropolar fluids," *Indiana University Mathematics Journal*, vol. 16, no. 1, pp. 1–18, 1966.

[3] A. H. Nayfeh, "Introduction to Perturbation Techniques," *ASME Journal of Heat Transfer*, vol. 107, no. 1, pp. 248–250, 1979.

[4] R. H. Rand and D. Armbruster, *Perturbation Methods, Bifurcation Theory and Computer Algebraic*, Springer, Berlin, Germany, 1987.

[5] A. Shehzad and R. Ali, "Approximate analytic solution for-magneto-hydrodynamic flow of a non-Newtonian fluid over a vertical stretching sheet," *Canadian Journal of Pure and Applied Sciences*, vol. 2, pp. 202–215, 2012.

[6] M. Turkyilmazoglu, "Some issues on HPM and HAM methods: a convergence scheme," *Mathematical and Computer Modelling*, vol. 53, pp. 1929–1936, 2011.

[7] T. Hussain, T. Hayat, S. A. Shehzad, A. Alsaedi, and B. Chen, "A model of solar radiation and joule heating in flow of third grade nanofluid," *Zeitschrift für Naturforschung A*, vol. 70, no. 3, pp. 177–184, 2015.

[8] S. J. Liao, *The proposed homotopy analysis technique for the solution of nonlinear problems*, PhD thesis, Shanghai Jiao Tong University, Shanghai, China, 1992.

[9] Z. Shah, M. Sheikholeslami, and P. Kumam, "Simulation of entropy optimization and thermal behavior of nanofluid through the porous media," *International Communications in Heat and Mass Transfer*, vol. 120, no. 8, Article ID 105039, 2021.

[10] Z Shah, E. Alzahrani, M. Jawad, and U. Khan, "Microstructure and inertial characteristics of MHD suspended SWCNTs and MWCNTs based maxwell nanofluid flow with bio-convection and entropy generation past a permeable vertical cone," *Coatings*, vol. 10, no. 10, p. 998, 2020.

[11] R. Alt and J. Vignes, "Validation of results of collocation methods for ODEs with the CADNA library," *Applied Numerical Mathematics*, vol. 21, no. 2, pp. 119–139, 1996.

[12] C. Franke and R. Schaback, "Solving partial differential equations by collocation using radial basis functions," *Applied Mathematics and Computation*, vol. 93, no. 1, pp. 73–82, 1998.

[13] C. Franke and R. Schaback, "Convergence order estimates of meshless collocation using radial basis functions," *Advances in Computational Mathematics*, vol. 8, no. 4, pp. 381–399, 1998.

[14] S. U. Siraj-ul-Islam, S. Haq, and A. Ali, "A meshfree method for the numerical solution of the RLW equation," *Journal of Computational and Applied Mathematics*, vol. 223, no. 2, pp. 997–1012, 2009.

[15] M. Uddin, S. Haq, and S. U. Siraj-ul-Islam, "Numerical solution of complex modified Korteweg-de Vries equation by mesh-free collocation method," *Computers & Mathematics with Applications*, vol. 58, no. 3, pp. 566–578, 2009.

[16] M. Uddin, S. Haq, and S. U. Siraj-ul-Islam, "A mesh-free numerical method for solution of the family of Kuramoto-Sivashinsky equations," *Applied Mathematics and Computation*, vol. 212, no. 2, pp. 458–469, 2009.

[17] S. Haq, S. U. Islam, and M. Uddin, "A meshfree method for the numerical solution of the KdVBurgers equation," *Applied Mathematical Modelling*, vol. 33, no. 8, pp. 3442–3449.

[18] S. Haq, S. U. Islam, and M. Uddin, "A meshfree interpolation method for the numerical solution of the coupled nonlinear partial differential equations," *Engineering Analysis with Boundary Elements*, vol. 33, no. 3, pp. 399–409, 2009.

[19] A.-M. Wazwaz, "Adomian decomposition method for a reliable treatment of the Bratu-type equations," *Applied Mathematics and Computation*, vol. 166, no. 3, pp. 652–663, 2005.

[20] H. Hameed, A. M. Siddiqui, B. M. Siddique, and Q. K. Ghori, "Use of adomian decomposition method in the study of parallel plate flow of a third grade fluid," *Communications in Nonlinear Science and Numerical Simulation*, vol. 15, no. 9, pp. 2388–2399, 2010.

[21] M. Cakmak and S. Alkan, "A numerical method for solving a class of systems of nonlinear Pantograph differential equations," *Alexandria Engineering Journal*, 2021.

[22] B. Sun, S. Wen, S. Wang, T. Huang, Y. Chen, and P. Li, "Quantized synchronization of memristive neural networks with time-varying delays via super-twisting algorithm," *Neurocomputing*, vol. 380, pp. 133–140, 2020.

[23] M. A. Zaky, "An accurate spectral collocation method for nonlinear systems of fractional differential equations and related integral equations with nonsmooth solutions," *Applied Numerical Mathematics*, vol. 154, pp. 205–222, 2020.

[24] D. Ziane, C. Mountassir Hamdi, C. Cattan, and K. Belghaba, "Yang-laplace decomposition method for nonlinear system of local fractional partial differential equations," *Applied Mathematics and Nonlinear Sciences*, vol. 4, no. 2, pp. 489–502, 2019.

[25] O. Moaaz, I. Dassios, O. Bazighifan, and A Muhib, "Oscillation theorems for nonlinear differential equations of fourth-order," *Mathematics*, vol. 8, no. 4, p. 520, 2020.

[26] S. R. Nekoo, "Model reference adaptive state-dependent Riccati equation control of nonlinear uncertain systems: regulation and tracking of free-floating space manipulators," *Aerospace Science and Technology*, vol. 84, pp. 348–360, 2019.

[27] H. Hassan and M. M. Rashidi, "An analytic solution of micropolar flow in a porous channel with mass injection using homotopy analysis method," *International Journal of Numerical Methods for Heat and Fluid Flow*, vol. 24, no. 2, 2014.

[28] I. Khan, M. A. Z. Raja, M. Shoaib et al., "Design of neural network with Levenberg-Marquardt and Bayesian regularization backpropagation for solving pantograph delay differential equations," *IEEE Access*, vol. 8, pp. 137918–137933, 2020.

[29] N. A. Kelson, A. Desseaux, and T. W. Farrell, "Micropolar flow in a porous channel with high mass transfer," *ANZIAM Journal*, vol. 44, pp. 479–495, 2003.

[30] A. Desseaux and N. A. Kelson, "Solutions for the flow of a micropolar fluid in a porous channel," in *Proceedings of the 4th Biennial Engineering Mathematics and Applications Conference*, pp. 115–118, Melbourne, Australia, September 2000.

[31] Z. Ziabakhsh and G. Domairry, "Homotopy analysis solution of micro-polar flow in a porous channel with high mass transfer," *Advances in Theoretical and Applied Mathematics*, vol. 1, pp. 79–94, 2008.

[32] M. M. Rashidi and E. Erfani, "A novel analytical method to investigate effect of radiation on flow of magneto micropolar fluid past a continuously moving plate with suction and injection," *International Journal of Modeling Simulation Scientific Computation*, vol. 1, no. 2, pp. 219–238, 2010.

[33] M. M Rashidi, S. A. M. Pour, and N Laraqi, "A semi-analytical solution of micro polar flow in a porous channel with mass injection by using differential transform method," *Nonlinear Analysis Modelling and Control*, vol. 15, no. 3, pp. 341–350, 2010.